Title
Changes in Structural Networks after Radiation Therapy in Patients with Brain Tumors

Author
Yeh, Joy

Publication Date
2016

Peer reviewed|Thesis/dissertation

Changes in Structural Networks after Radiation Therapy in Patients with Brain Tumors

by

Joy Yeh

THESIS

Submitted in partial satisfaction of the requirements for the degree of

MASTER OF SCIENCE

in

Biomedical Imaging

in the

GRADUATE DIVISION

of the

UNIVERSITY OF CALIFORNIA, SAN FRANCISCO

Acknowledgements

This project was made possible by a committee of incredible individuals who spent countless hours, days, weeks, and months to help a student grow. I'd like to thank Dr. Xu and Dr. Lupo for having the faith to give me such a wonderful opportunity at a time when my interest in MRI was newly minted and fresh, and continuing to help me as I worked through the inevitable problems along the way. I'd like to thank Dr. Hess for being an amazing educator and inspiring a love for diffusion MRI and mathematical applications. I'd like to thank Dr. Tymofiyeva for her dedication to education, extraordinary patience, unyielding positive energy, and genuine good nature. To say that this project would not have come together without her help is an understatement, and I've lost count how many ways she has gone above and beyond expectations in contributing her effort, time, and support.

I'd also like to thank Dr. Saloner, Dr. Martin, and the MSBI administrators for all their efforts throughout the year. And finally, thank you to the classmates that have helped me through important decisions and made this program enjoyable.

Changes in Structural Networks after Radiation Therapy in Patients with Brain Tumors

by Joy Yeh

Introduction - Radiation therapy (RT) received by brain tumor patients after tumor resection can affect brain connectivity in various degrees. Structural connectivity changes in brain matter can be modeled by diffusion MRI and tractography between areas of the brain that act as nodes of the network. We hypothesize that graph theory measures, including global network descriptors and local node characteristics, may change with the application of radiation therapy and evolve over time.

Methods - Six patients with brain tumor resections were imaged either before or immediately following RT and then again six months later. Diffusion data were registered with a brain atlas (AAL), and post-gad T1- and T2-weighted FLAIR images were clinically marked for tumor-affected tissues. Networks were constructed using 90 AAL regions as nodes and connecting streamlines as edges, weighted by the average fractional anisotropy (FA) within those streamlines. Four global and four local network measures were examined. Tumor-affected node sets were defined in each patient and examined for changes, then compared against contralateral nodes and all non-affected nodes. Obtained network measures were correlated with cognitive data.

Results - Network average clustering coefficient increased significantly between scans ($p=0.0313$). Local clustering, local efficiency, and node strength showed increasing trends in selected node sets. Node strength increased significantly with T1 and T2 image-based definitions of tumor-affected nodes six months post-RT in a single patient. Correlation was detected between cognitive scores and betweenness centrality in select tumor-affected nodes.

Conclusions - Several connectivity measures appeared to be altered in patients after radiation therapy in a span of six months, including increases in network average clustering. Small sample size limited the level of confidence of observed changes in local measures and correlation to cognitive scores but suggests connectivity changes in tumor-affected regions and betweenness centrality in relation to cognitive scores as points of interests in future studies.

Contents

List of Tables

List of Figures

List of Symbols

N	set of all nodes in a network
n	number of nodes in a network
(i, j)	link between nodes i and j $(i, j \in N)$
$w_{i,j}$	weight of edge between nodes i and j $(i, j \in N)$, normalized such that $0 \leq w_{i,j} \leq 1$
k_i	weighted degree of node i, such that $k_i = \sum_{j \in N} w_{i,j}$
d_{ij}	shortest weighted path length between i and j, $d_{ij} = \sum_{w_{ij}^{-1} \in g_{i \leftrightarrow j}} f(w_{uv})$ where f is an inverse map from weight to length and $g_{i \leftrightarrow j}$ is the shortest weighted path between i and j
t_i	weighted geometric mean of triangles around i, $t_i = \frac{1}{2} \sum_{j,h \in N} (w_{ij} w_{ih} w_{jh})^{1/3}$
ρ_{hj}	the number of shortest paths between i and j, and $p_{hj}(i)$ is the number of shortest paths between h and j that pass through i

Dedicated to my grandfather,
an engineer and physician

Chapter 1

Introduction

1.1 Motivation

Standard of care for patients with high grade gliomas currently includes tumor resection followed by radiation therapy and chemotherapy (Stupp et al., 2007). Previous literature suggests that radiation therapy may affect brain tissue by demyelination, mild structural degradation of axonal fibers, and microbleeds in tissues (Nagesh et al., 2008; Lupo et al., 2012) Changes in these tracts may alter brain function through interruption or changes in the network. Structural connectomes can be used to study the white matter tract connections of the human brain; until recently, few applications of this method have been performed to examine the effects of radiation therapy on structural connectivity (Sporns, Tononi, and Kötter, 2005). Such an analysis may provide new insights into the effects of radiation therapy on the brain and may offer guidance in future treatment strategies.

1.2 Background

Patients with malignant high-grade gliomas undergo radiation therapy and chemotherapy treatment following surgical removal of tumors. The effects of radiation therapy have been known to be detrimental, with studies noting microbleeds in tissues years after application of radiation (Lupo et al., 2012). Although a multitude of connectome studies have been performed, very few studies have applied this methodology to investigate the effects of radiation therapy.

Connectome analysis examines the network of connections in the brain. These studies are segregated into analysis of the functional and structural connectome (Sporns, Tononi, and Kötter, 2005). Functional networks are derived from fMRI studies and are based on temporal activation measured by Blood-Oxygen-Level Dependent (BOLD) response (Biswal et al., 2010). Previous functional connectome studies have found connectivity alterations that correlated significantly to changes in cognitive scores in attention in the context of radiation therapy in nasopharyngeal carcinoma patients, with particular changes in attention (Ma et al., 2016).

In contrast, structural connectomes are based on physical connections of white matter tracts in a network between brain regions and are derived from diffusion MRI (Sporns, Tononi, and Kötter, 2005). Structural connectome changes have been studied extensively for various conditions, including but not limited to epilepsy, dementia, schizophrenia, multiple sclerosis, and development in children, with various changes (Griffa et al., 2013; Tymofiyeva et al., 2014). However, fewer studies have analyzed structural networks in relation to cancer and radiation therapy. One study of structural connectivity in adult patients who had been treated for brain tumors as children noted variation in connectivity in relation to attention networks (Smith et al., 2014). The effects of chemotherapy on connectivity in leukemia patients have included lower network average clustering, among other changes (Kesler et al., 2016). In patients with pediatric medulloblastoma, a decrease in FA was found 12 weeks after radiation therapy ended (Duncan et al., 2016). Though related in methodology, an evaluation of structural changes in adult patients with high-grade gliomas may describe underlying changes occurring during radiation application in fully developed brains.

1.2.1 Diffusion MRI

In white matter, cellular membranes of the myelin sheath restrict water diffusion orthogonal to the fibers. Diffusion Weighted Imaging (DWI) uses diffusion sensitizing gradients to highlight the diffusion of water during the imaging sequence. Diffusion Tensor Imaging (DTI) models the diffusion magnitude, anisotropy and orientation as a tensor. DTI measures include fractional anisotropy (FA), which describes the degree of anisotropy of a diffusion process and may be determined from the tensor. FA values are generally high in white matter tracts, lower with degradation, and can indicate structural integrity of fibers (Melhem et al., 2002). DTI uses a spin echo pulse sequence with diffusion gradients and echo planar imaging readout (EPI) in a minimum of 6 non-collinear directions to describe the diffusion tensor. Such scans also utilize a b=0, or b0 reference scan where no diffusion-sensitizing gradients are applied. Some post-processing such as eddy-current corrections may be based off of the b0 scan and multiple b0 scans captured throughout the scan, theoretically allowing for additional motion correction. Greater b values, reflecting the application of diffusion gradients, allow for greater diffusion weighting to detect slower diffusion processes (Mukherjee et al., 2008).

High Angular Resolution Diffusion Imaging (HARDI) allows for better delineation of white matter tracts by addressing crossing tracts compared to standard DTI by using a higher order of modeling, utilizing additional directions with higher b-values (Hess et al., 2006). Q-ball reconstruction allows for resolution of multiple intravoxel fiber orientation (Tuch, 2004). Selection of HARDI data to use may require rejection of directions in which eddy currents and other artifacts affect image quality. FA and primary eigenvectors are known to be affected by rejection of directions (Chen et al., 2015).

1.2.2 Anatomical Images

Within each patient, different sets of tumor-affected tissues may be identified depending on MRI scan parameters. T2-weighted FLAIR images may show a combination of infiltrative tumor and edema as hyperintense regions while suppressing cerebrospinal fluid signal. T1-weighted images after the injection of gadolinium-based contrast agent depict necrosis and areas of breakdown of the blood-brain barrier (Just and Thelen, 1988). Use of contrast agents with T1-weighted images allows for detection of potential inflammation or breakdown of the blood-brain barrier. Tumor-affected areas may include these contrast-enhanced lesions (CEL), as well as the surrounding non-enhancing T2 lesions (NEL) (Graif et al., 1985).

1.2.3 Network Analysis

A graph is defined as a set of nodes and edges (connections) between them. Connections can be obtained from diffusion MRI and tractography. Application of atlases such as the Automated Anatomical Labeling (AAL) atlas allows for parcellation of the brain to regions that act as nodes (Heckemann et al., 2006). A graph can be represented as a connectivity matrix where entries relate to the connections between two parcels within the brain and act as edges. These edges can be weighted and carry values relating to the level of connectivity between the nodes, or brain regions they connect. Registration of data to a common atlas and template space allows consistency despite anatomical variations between patients (Klein et al., 2009).

Graph theory measures of the resulting networks may include both global measures that describe the network as a whole and local measures particular to individual nodes (Bullmore and Sporns, 2009). Global measures include network average clustering coefficient (C), characteristic path length (L), small world index (S), and transitivity (T) (Rubinov and Sporns, 2010). Local measures include local clustering coefficient (c_i), local efficiency (e_i), node strength (s_i), and betweenness centrality (b_i) (Rubinov and Sporns, 2010).

The network average clustering coefficient reflects the local clustering at each node (Sporns et al., 2004). Similarly, the characteristic path length is a reflection of the inverse of the global efficiency of the network (Bullmore and Sporns, 2009). In the case of brain tumors, the changes in specific nodes may be of interest in addition to the overall network measure. Some of these measures, such as clustering and transitivity examine the connectivity between node neighbors (Sporns et al., 2004). Transitivity places more weight on high degree nodes whereas the network average clustering coefficient evaluates low degree nodes with the same weight (Rubinov and Sporns, 2010). Characteristic path length, local efficiency, and node strength are more indicative of weights in connections (throughout the network, in local networks of individual nodes, and in connection to a single node, respectively) rather than patterns of node linkage, and

reflect physiological efficacy (He and Evans, 2010). Small world indices evaluate a specific pattern of connection described by networks with node connections to few neighbors and efficient traversal between node pairs. Bassett and Bullmore have described this phenomenon as a measure of "cost-effectiveness" in natural connected networks (Bassett and Bullmore, 2006). Finally, betweenness centrality of individual nodes is of interest in the cases of brain tumors since it reflects the number of shortest paths (and thereby the most efficient paths) through a particular node. This measure may be expected to increase with function and usage of a particular node and decrease with use of alternative paths of network traversal (Alstott et al., 2009).

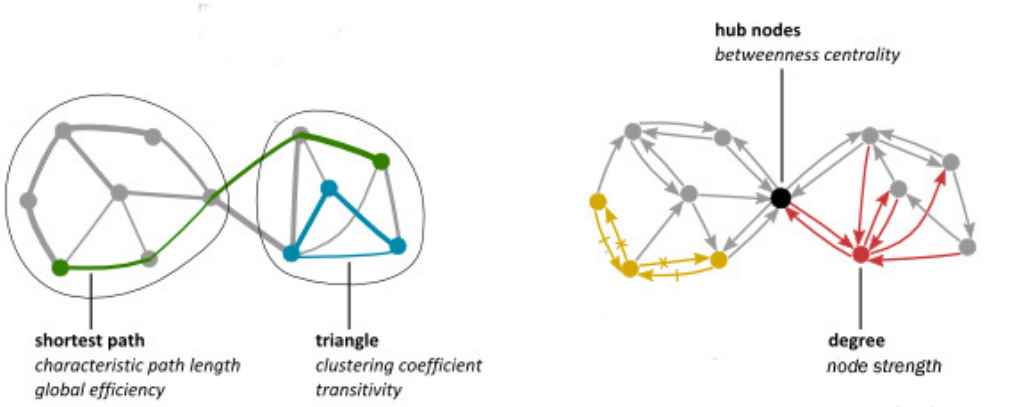

FIGURE 1.1: Network measures describe graphs of nodes and edges. Adapted from Rubinov M, Sporns O (2010) NeuroImage 52:1059-69

1.2.4 Cognitive Scores

Previous studies have shown radiation therapy may cause changes in cognitive function, which is linked to degradation of white matter structural integrity (Aoyama et al., 2007). The Montreal Cognitive Assessment (MoCA) tests short term recall, visuospatial abilities, executive function, attention, concentration, working memory, and orientation to time and place (Nasreddine et al., 2005). Cognitive tests may include memory, language, executive function, visual-spatial, and visual-motor speed scores, combined with behavioral and quality of life tests into a total score that measures overall performance as a total or global z-score. While relatively little is known about these changes in the context of radiation therapy and effects on underlying white matter tracts, a structural connectivity study may provide new insights in this area.

1.3 Project Goals

We hypothesize that changes in structural connectivity in brain tumor patients will take place after treatment with radiation therapy and seek to investigate differences through network analysis of global and local properties.

Chapter 2

Methods

2.1 Data Acquisition

Data was obtained from six high grade glioma patients (grades III-IV) who were imaged using a GE Medical Systems Signa HDx 3.0T scanner at the University of California, San Francisco. Images were obtained after surgical tumor resection but either immediately before (4 patients) or after (2 patients) radiation therapy, and again after six months, during which patients were treated with radiation therapy and adjuvant chemotherapy. These scans will be referred to as pre-RT scans and post-RT scans, respectively. These images had voxel size 1.094 x 1.094 x 2.600 mm and 256 x 256 x 44 matrix, obtained with 55 diffusion directions (HARDI) and 7 b_0 image set volumes, with a maximum b value of 2000 s/mm^2. Additionally, T2 FLAIR and pre/post-gad T1 SPGR MRI images were obtained for anatomical reference.

2.2 Pre-processing

An automatic data rejection algorithm was used to discard corrupted image set volumes affected by motion. These images were identified as outliers with signal intensity ripples or loss. Images that exceeded a threshold number of pixels deviating from mean pixel value for all diffusion directions by three standard deviations or more were labeled as corrupt. The threshold for number of pixels was set based on head size. Slices corresponding to areas including and inferior to the nasal cavities, as well as those corresponding to the superior edge were excluded, as defined by the lower 1/3 and top 1/6 slices, respectively. The six additional b_0 image set volumes were also discarded due to Diffusion Toolkit (Wang et al., 2007) restriction on input formatting of data files.

2.3 Tractography

Tractography was performed using Diffusion Toolkit and reconstructed for streamlines in DTI space. In the case of DTI reconstruction, the deterministic Fiber Assignment by Continuous Tracking (FACT) algorithm was applied using the entire diffusion-weighted image set volume as the mask image (Mori et al., 1999) . A threshold angle of

35^o was chosen as a compromise between false positive and false negative streamlines (Moldrich et al., 2010) . Trackvis was used for visualization (Wang et al., 2007).

2.4 Registration and Parcellation

DTI data were registered to the MNI space template after application of Brain Extraction Tool (BET) (Smith, 2002) . FA maps were registered to the standard FMRIB58_FA_1mm atlas in MNI space using FLIRT (Jenkinson and Smith, 2001; Jenkinson et al., 2002) . Subsequent registration to DTI space was performed to match tractography. Application of the Automated Anatomical Labeling (AAL) atlas to diffusion data was performed with registration of parcel regions of interest (ROIs) to MNI then to DTI space for definition of network nodes using FLIRT and Matlab 2015b (Tzourio-Mazoyer et al., 2002; MATLAB, 2015) Nodes were identified using backwards mapping of image intensities to parcels. 90 AAL parcels were selected for examination. Parcels of the cerebellum were excluded.

2.5 Matrix Generation

Weighted undirected connectivity matrices were constructed through Matlab for each scan. For each graph represented by a matrix, 90 AAL parcellations acted as nodes, or vertices, to represent known brain regions. For each edge $e_{i,j}$ connecting a pair of nodes v_i and v_j, the average FA within voxels through which tractography streamlines passed between nodes v_i and v_j, were used to generate edge weight values. Node volumes were also calculated.

2.6 Global Measures

Global properties of network average clustering coefficient, characteristic path length, small world index, and transitivity were derived as a network-wide value for each scan using Matlab and the Brain Connectivity Toolbox for comparison of measures in pre-RT and post-RT scans (Rubinov and Sporns, 2010). These measures are based on the following graph theory concepts and definitions, adapted from Rubinov and Sporns (Bullmore and Sporns, 2009). Refer to List of Symbols for definitions and figure 1.1 for visualization.

The network average clustering coefficient is a measure of segregation and is a measure of how connected node neighbors are to each other (Onnela et al., 2005). In the context of connectome analysis, the network average clustering coefficient was used characterize connectivity changes on a smaller scale than some of the other network measures, averaged across all nodes in the network. The network average clustering coefficient is defined as

$$C = \frac{1}{n} \sum_{i \in N} \frac{2t_i}{k_i(k_i - 1)} \tag{2.1}$$

The characteristic path length describes the shortest paths, or summation of inverted edge weights for all possible pairs of nodes in a network, averaged over the entire set of edges (Watts and Strogatz, 1998). This measure was used as an assessment of overall integration. Weighted characteristic path length is defined as

$$L = \frac{1}{n} \sum_{i \in N} \frac{\sum_{j \in N, j \neq i} d_{ij}}{n - 1} \tag{2.2}$$

Small world indices evaluate the characteristic of the graph where nodes have few neighbors but most pairs of nodes can be accessible through short paths. The mathematical evaluation of this index compares ratios of clustering and characteristic path length to their respective randomized values on the same networks (Humphries and Gurney, 2008). The small world index is defined as

$$S = \frac{C/C_{rand}}{L/L_{rand}} \tag{2.3}$$

Transitivity is the ratio of triangles to triplets in the network, where triplets are three connected nodes (therefore each triangle contains three triplets). Like the clustering coefficient, transitivity is a segregation measure and reflects changes in connectivity on smaller scales (Newman, 2003). Weighted transitivity is defined as

$$T = \frac{\sum_{i \in N} 2t_i}{\sum_{i \in N} k_i(k_i - 1)} \tag{2.4}$$

For each global measure, the Wilcoxon ranked sum test was applied between groups of patient scores before radiation, and patient scores after radiation.

2.7 Local Measures

Local properties of of local clustering coefficient, local efficiency, node strength, and betweenness centrality were derived for each scan using Matlab and the Brain Connectivity Toolbox for comparison of measures in pre-RT and post-RT scans (Rubinov and Sporns, 2010). These measures are calculated for each node and are based on the following graph theory concepts and definitions, adapted from Rubinov and Sporns (Bullmore and Sporns, 2009). Refer to Appendix A for definitions and figure 1.1 for visualization.

Local clustering coefficients characterize connections of individual nodes' neighbors. The network average clustering coefficient is derived from an average of these values (Onnela et al., 2005). Weighted local clustering coefficient is defined as

$$c_i = \frac{2t_i}{k_i(k_i - 1)} \tag{2.5}$$

Local efficiency is the summation of edge weights across all pairs of nodes in a local neighborhood (Bullmore and Sporns, 2009). Weighted local efficiency is defined as

$$e_i = \frac{1}{n}\sum_{i\in N}\frac{\sum_{j,h\in N, j\neq i}(w_{ij}w_{ih}[d_{jh}(N_i)]^{-1})^{1/3}}{k_i(k_i-1)} \tag{2.6}$$

Node strength reflects the connectivity of a node i as the sum of weights in all edges connected to node i (Hagmann et al., 2010). For each node i, node strength is defined as

$$s_i = \sum_{j\in N} w_{ij} \tag{2.7}$$

Betweenness centrality is the fraction of all shortest paths in the network that contain a given node. For nodes that are included in larger numbers of shortest path connections, this value will be higher (Freeman, 1978). Betweenness centrality is defined as

$$b_i = \frac{1}{(n-1)(n-2)}\sum_{h,j\in N, h\neq j, h\neq i, j\neq i}\frac{\rho_{hj}(i)}{\rho_{hj}} \tag{2.8}$$

2.8 Node Set Definition

The T2-hyperintense lesion (T2L) and contrast enhancing lesion (CEL) were generated from coregistered T2 FLAIR MRI images and post-gad T1 MRI images, respectively. Masks were created for these voxels and registered to DTI space to match each scan using FLIRT. Nodes whose parcel volumes included the masked tumor-affected areas (CEL and T2) were selected for local analysis, heretofore referred to as the tumor-affected nodes. A set of non-enhancing lesion (NEL) nodes was also defined by subtracting the T2L and CEL masks.

In cases where pre-RT scans and post-RT scans identified slightly different sets of tumor-affected nodes for local analysis (<10 unique nodes per patient), the union of these sets of node was used for data analysis. All nodes not labeled tumor-affected, or normal (Non) were also identified as a comparative set, for a total of 5 sets of nodes per patient.

2.8.1 Analysis Between Scans

Changes in measures were examined between scans. For each node set, the Wilcoxon signed rank test was then applied to compare post-RT to pre-RT local measures (averaged within patient-wise node sets) to find differences in node sets changes (defined as all nodes, non-tumor nodes, CEL nodes, T2L nodes, and NEL nodes) among all patients. These changes were also derived per patient for observation of direction of changes.

2.8.2 Analysis Between Tissues

Changes in measures were examined between tumor-affected and normal tissue. For each tumor-affected definition (CEL, T2L, NEL), the Wilcoxon rank sum was applied to compare tumor-affected to normal local measures (averaged as changes within patient-wise node sets) to find differences in tumor-affected node set changes (compared to normal tissue change) among all patients. These changes were also derived per patient for observation of direction of differences in changes.

2.9 Cognitive Correlates

MoCA and global z-scores were obtained as cognitive measures. These measures were compared with Spearman correlations across each of the 6 patients where each global measure and each average node set change for each local measure were tested as explanatory variables.

Chapter 3

Results

3.1 Processed Data

Automatic corrections resulted in less than 5 directions rejected per scan, with 8 scans resulting in no rejections. Tractography and registration results appeared reasonable despite some miscellaneous streamlines near the posterior and some minor registration mismatches especially near the anterior surface.

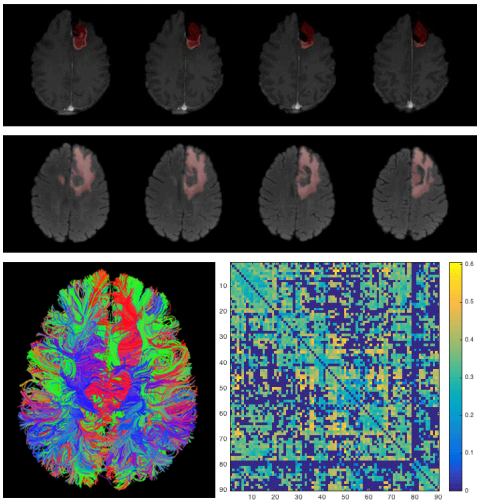

FIGURE 3.1: Samples from patient 5 pre-RT scan, clockwise from top: registered CEL and T2L masks; connectivity matrix weighted by FA between a 90 AAL-parcelled brain node network; tractography streamlines

3.2 Global Measures

Comparisons between pre-RT and post-RT scans showed general increases in network average clustering coefficients, and transitivity, decreases in characteristic path length, and little change in small world indices, shown in table 1. Significant increases were observed in network average clustering coefficients (p=0.031), whereas decreases in characteristic path length and increases in transitivity showed less consistent results. Refer to figure 3.2.

	Average Change	p-value
Network Avg Clustering	0.0133	0.0313
Characteristic Path Length	-0.0109	0.1563
Small World Index	0.0048	0.6991
Transitivity	0.0088	0.1563

TABLE 3.1: Global measures significantly increased in network average clustering coefficient (p=0.0313) when comparing paired pre-RT to post-RT scans.

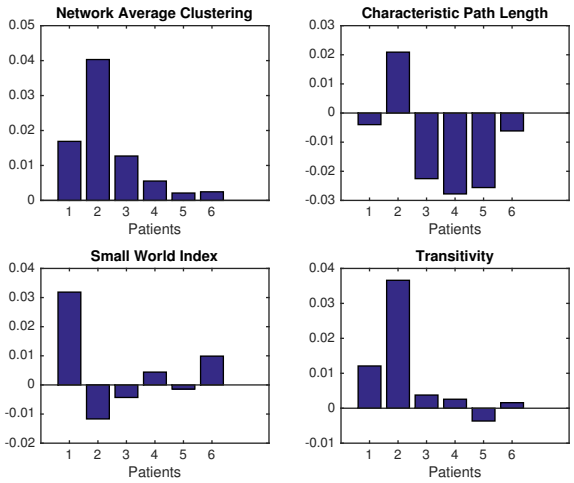

FIGURE 3.2: Global measures showed significantly increased network average clustering

3.3 Local Measures

3.3.1 Analysis Between Scans

Comparisons between pre-RT and post-RT scans showed general increases in local measures, shown in table 3.2. Significant increases were observed in several comparisons between larger groups of node sets (patient 2, for example had a tumor that included 54 out of 90 CEL nodes and 45 out of 90 T2L nodes). Refer to figure 3.3 and 3.4. Across all patients, each node set appeared to increase in local clustering, local efficiency, and node strength, with betweenness centrality showing less consistency. No changes appeared significant, however.

	All	Non	CEL	T2	NEL
Local Clustering	0.1797	0.4848	0.1320	0.2403	0.1320
Local Efficiency	0.9372	0.9372	0.8182	0.5887	0.5887
Node Strength	0.2403	0.3095	0.3939	0.4848	0.2403
Betweenness Centrality	0.5887	1.0000	0.3939	0.9372	0.2403

TABLE 3.2: Comparisons between post-RT and pre-RT (mean node set measures), observed across all patients as Wilcoxon rank sum test p-values

	All	Non	CEL	T2	NEL
Local Clustering	0.0133	0.0120	0.0148	0.0156	0.0164
Local Efficiency	0.0060	0.0049	0.0069	0.0075	0.0086
Node Strength	1.1840	0.9872	1.2768	1.1596	2.0343
Betweenness Centrality	2.0340	0.7999	1.6598	-0.0543	9.5615

TABLE 3.3: Comparisons between post-RT and pre-RT (mean node set measures), observed across all patients as mean differences

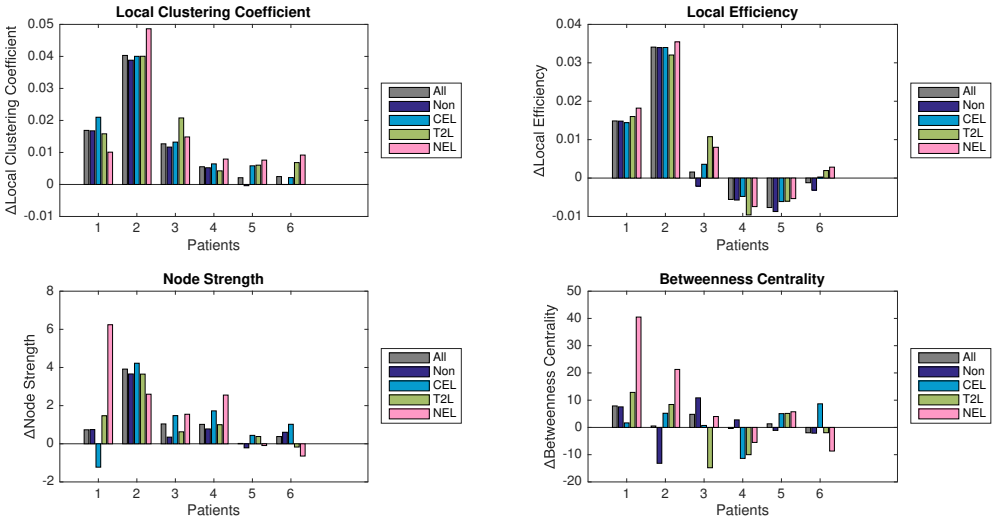

FIGURE 3.3: Grouped by patient - node sets showed overall increases in local clustering, local efficiency, and node strength averages among each node set. Betweenness centrality showed more variation.

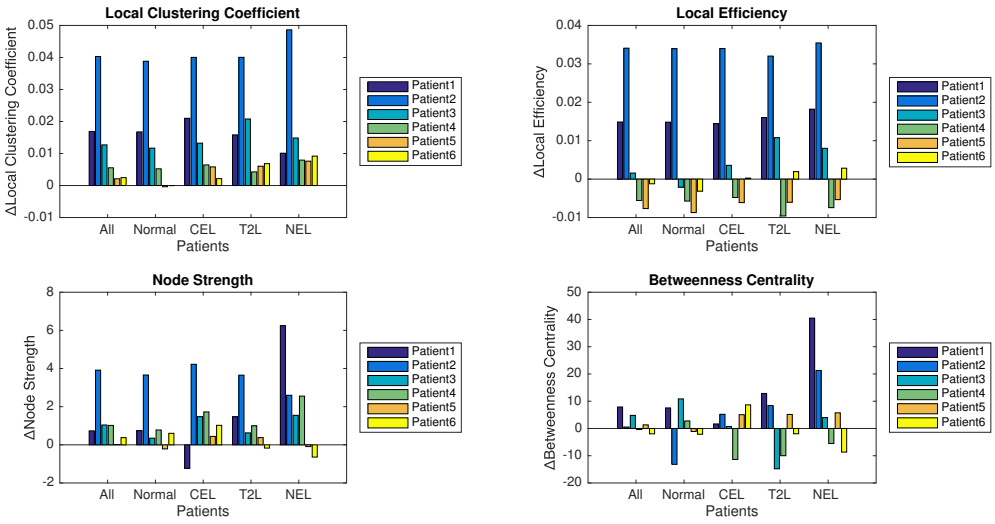

FIGURE 3.4: Grouped by node set - node sets showed overall increases in local clustering, local efficiency, and node strength averages among each node set. Betweenness centrality showed more variation.

3.3.2 Analysis Between Tissues

Comparisons between tumor-affected and normal tissues showed generally more positive changes in local clustering, local efficiency, node strength than normal tissues, shown in table 3.4 and 3.5. Significant differences were observed in patient 5 whose average node strength in CEL and T2L node sets increased significantly more in comparison to normal nodes (whose average node strengths decreased). Refer to figure 3.5 and 3.6. Across all patients, non-enhancing lesions appeared to increase more in local clustering than normal tissue (p=0.0457) and decrease more in betweenness centrality than normal tissue (p=0.1517). Both these changes were seen at nonsignificant levels when accounting for Bonferroni corrections. Strength and power of these observations will be discussed further.

	CELvNT	T2vNT	NELvNT
Local Clustering	0.7259	0.0971	0.0457
Local Efficiency	0.5456	0.3051	0.3292
Node Strength	0.7259	0.4412	0.3012
Betweenness Centrality	0.9643	0.2688	0.1527

TABLE 3.4: Comparisons between tumor-affected and normal tissue (mean node set measure changes), observed across all patients as Wilcoxon signed rank p-values

	CELvNT	T2vNT	NELvNT
Local Clustering	0.0022	0.0069	0.0092
Local Efficiency	0.0034	0.0051	0.0060
Node Strength	0.4183	-0.7749	-1.2479
Betweenness Centrality	10.7879	0.1733	-6.5455

TABLE 3.5: Comparisons between tumor-affected and normal tissue (mean node set measure changes), observed across all patients as mean differences

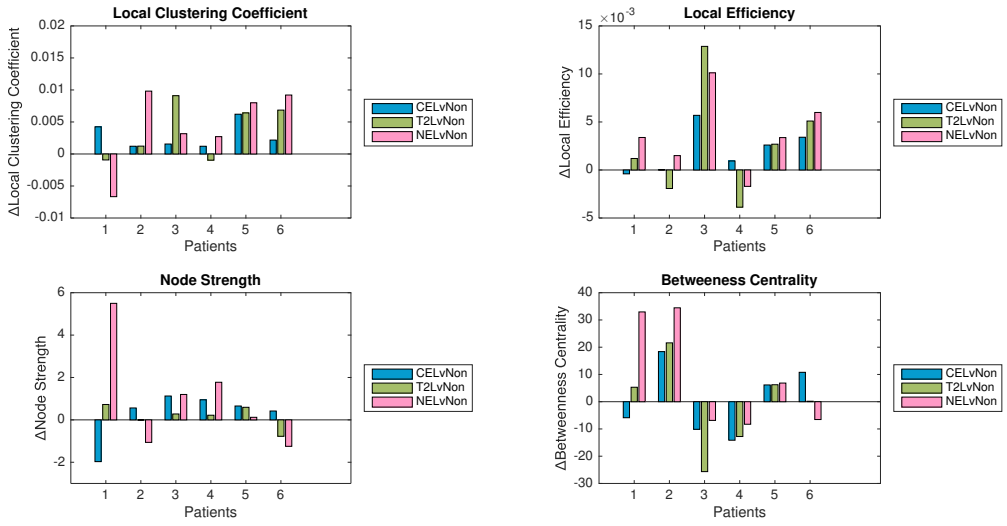

FIGURE 3.5: Grouped by patient - tumor-affected nodes showed nonsignificant increases in local clustering and decreases in betweenness centrality when comparing non-enhancing lesions to normal tissue.

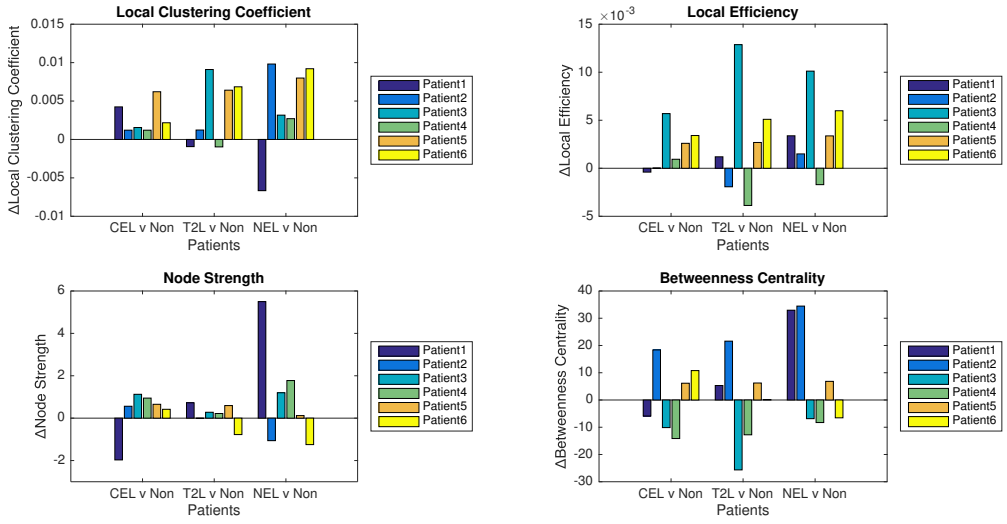

FIGURE 3.6: Grouped by comparisons - tumor-affected nodes showed nonsignificant increases in local clustering and decreases in betweenness centrality when comparing non-enhancing lesions to normal tissue.

3.4 Cognitive Correlates

Cognitive scores either improved or remained unchanged overall and showed non-significant correlations betweenness centrality and global z-score (p=0.0165). Refer to tables 3.6-3.8 and figures 3.7-3.8.

	MoCA	Global-z
Local Clustering	0.8465	0.1684
Local Efficiency	0.7807	0.0705
Node Strength	0.6855	0.3556
Betweenness Centrality	0.9072	0.1548

TABLE 3.6: P-valeus of correlation of global measures to cognitive scores.

MoCA	Normal	CEL	T2	NEL
Local Clustering	0.8134	0.7530	0.6709	0.8385
Local Efficiency	0.9382	0.8621	0.5716	0.7009
Node Strength	0.6006	0.4149	0.9480	0.4129
Betweenness Centrality	0.1447	0.8833	0.9576	0.2931

TABLE 3.7: P-values of correlation of local measures to MoCA scores.

Global-z	Normal	CEL	T2	NEL
Local Clustering	0.1641	0.1222	0.2439	0.3792
Local Efficiency	0.0562	0.0703	0.0679	0.0508
Node Strength	0.3179	0.7880	0.2344	0.1422
Betweenness Centrality	0.6941	0.4024	0.0482	*0.0165*

TABLE 3.8: P-values of correlation of local measures to global z-scores shows non-significant correlation of global z-score to betweenness centrality in NEL nodes.

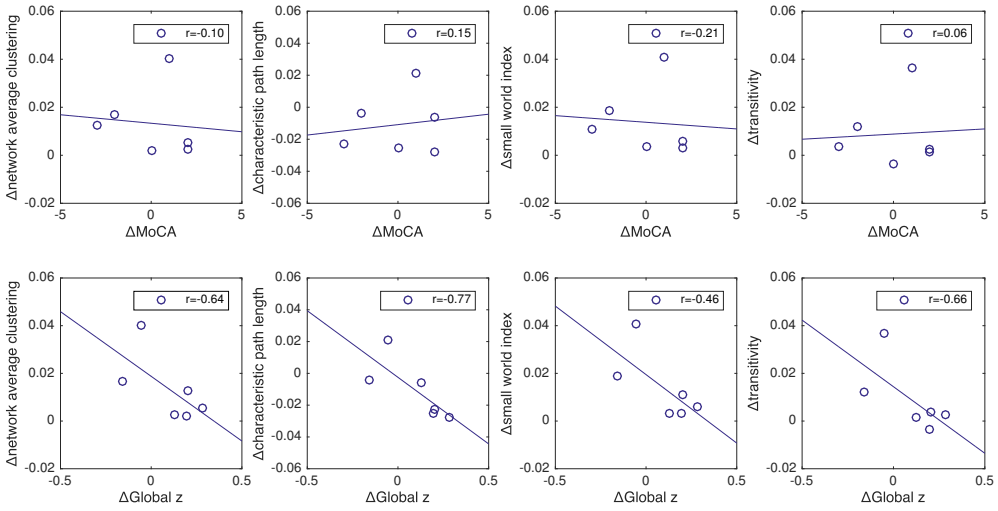

FIGURE 3.7: Correlation of global measures to cognitive scores with rho values

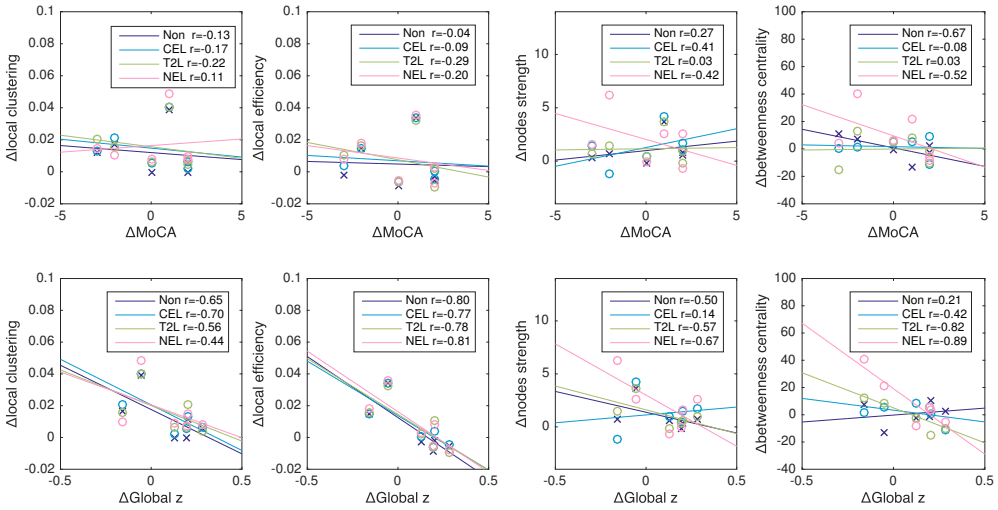

FIGURE 3.8: Correlation of local measures to cognitive scores with rho values

Chapter 4

Discussion

4.1 Global Measures

The changes observed in network average clustering coefficient were somewhat surprising in that they implied improvement rather than degradation after radiation therapy ($p=0.0313$). These changes may be reflective of rewiring and recovery of tissues over time. Though falling short of significant ($p=0.1563$), the decrease in characteristic path length (indicating an increase in global efficiency) may be of interest in future studies with more power.

4.2 Local Measures

Average changes between scans within patient-wise node sets showed several significant changes in comparisons that included larger node sets, supporting global results and implications of general improvement. Lack of significance in examination of these changes across all patients may be due to the limiting factor of having only six patients.

Significant differences in patient 5 between CEL and T2L average node strength is unexplained. In examining the tumor sizes, patient 5 appears to have more nodes included in the post-scan compared to pre-scan. The difference between groups also appears somewhat uncharacteristic when compared against the same difference in other patients. Further analysis and if available, additional data such as radiation dosage maps may be needed to better explain this observation.

In comparisons between tissue types among all patients, local clustering in non-enhancing lesions may be of interest to observe in future studies with greater power ($p=0.0457$), given the restriction of Bonferroni corrections and small number of patients in this study.

4.3 Cognitive Scores

Similarly, the correlation of betweenness centrality and global z-score brings up a potential aspect of future exploration. The implication of negative correlation of betweenness centrality and cognitive scores in non-enhancing tumor-affected areas may suggest improvements when rewiring occurs through alternative pathways, while rewiring through the affected area worsens function. This is partially supported by soft evidence of negative correlation in CEL and T2 definitions of tumor-affected tissues and positive correlation of normal tissue to global z-score, where an increase in alternative pathways would increase betweenness centrality of normal tissue nodes. Nonetheless, a general increase in cognitive scores supports the improvements observed in network average clustering and efficiency in this time scale. In contrast to the previous study that investigated pediatric medulloblastoma at a 12 week time scale (Duncan et al., 2016), 6 months may be more conducive to rewiring and repair in white matter tracts.

4.4 Limitations

As an exploratory study, the results suggest some measures as potential points of interests for future studies with a larger number of subjects. Caution should be taken since the obtained results are based on a small number of patients upon which many calculations have been made, not precluding chance of coincidental significant findings. This study did not examine subnetworks of nodes, but future studies may be able to correlate changes in measure in subnetwork relating to particular cognitive function and corresponding cognitive scores. Future use of smaller parcellations may allow for better categorization of nodes into tumor-affected and normal tissues. Alternate definitions of node categories may also provide more detailed results specific to the biological state of tissues. Further examination may also be able to correlate radiation dosage map scores to local measures.

Chapter 5

Conclusion

Several structural brain connectivity measures appeared to be altered in patients after radiation therapy in a six month timeline, including significant increases in network average clustering. Small sample size limits the level of confidence of observed changes but suggests several directions for future studies.

Bibliography

Alstott, Jeffrey et al. (2009). "Modeling the impact of lesions in the human brain". In: *PLoS Comput Biol* 5.6, e1000408.

Aoyama, Hidefumi et al. (2007). "Neurocognitive function of patients with brain metastasis who received either whole brain radiotherapy plus stereotactic radiosurgery or radiosurgery alone". In: *International Journal of Radiation Oncology* Biology* Physics* 68.5, pp. 1388–1395.

Bassett, Danielle Smith and ED Bullmore (2006). "Small-world brain networks". In: *The neuroscientist* 12.6, pp. 512–523.

Biswal, Bharat B et al. (2010). "Toward discovery science of human brain function". In: *Proceedings of the National Academy of Sciences* 107.10, pp. 4734–4739.

Bullmore, Ed and Olaf Sporns (2009). "Complex brain networks: graph theoretical analysis of structural and functional systems". In: *Nature Reviews Neuroscience* 10.3, pp. 186–198.

Chen, Yiran et al. (2015). "Effects of rejecting diffusion directions on tensor-derived parameters". In: *NeuroImage* 109, pp. 160–170.

Duncan, Elizabeth C et al. (2016). "Application of probabilistic fiber-tracking method of MR imaging to measure impact of cranial irradiation on structural brain connectivity in children treated for medulloblastoma". In: *SPIE Medical Imaging*. International Society for Optics and Photonics, 97882Q–97882Q.

Freeman, Linton C (1978). "Centrality in social networks conceptual clarification". In: *Social networks* 1.3, pp. 215–239.

Graif, Moshe et al. (1985). "Contrast-enhanced MR imaging of malignant brain tumors." In: *American journal of neuroradiology* 6.6, pp. 855–862.

Griffa, Alessandra et al. (2013). "Structural connectomics in brain diseases". In: *Neuroimage* 80, pp. 515–526.

Hagmann, Patric et al. (2010). "White matter maturation reshapes structural connectivity in the late developing human brain". In: *Proceedings of the National Academy of Sciences* 107.44, pp. 19067–19072.

He, Yong and Alan Evans (2010). "Graph theoretical modeling of brain connectivity". In: *Current opinion in neurology* 23.4, pp. 341–350.

Heckemann, Rolf A et al. (2006). "Automatic anatomical brain MRI segmentation combining label propagation and decision fusion". In: *NeuroImage* 33.1, pp. 115–126.

Hess, Christopher P et al. (2006). "Q-ball reconstruction of multimodal fiber orientations using the spherical harmonic basis". In: *Magnetic Resonance in Medicine* 56.1, pp. 104–117.

Humphries, Mark D and Kevin Gurney (2008). "Network 'small-world-ness': a quantitative method for determining canonical network equivalence". In: *PloS one* 3.4, e0002051.

Jenkinson, Mark and Stephen Smith (2001). "A global optimisation method for robust affine registration of brain images". In: *Medical image analysis* 5.2, pp. 143–156.

Jenkinson, Mark et al. (2002). "Improved optimization for the robust and accurate linear registration and motion correction of brain images". In: *Neuroimage* 17.2, pp. 825–841.

Just, M and M Thelen (1988). "Tissue characterization with T1, T2, and proton density values: results in 160 patients with brain tumors." In: *Radiology* 169.3, pp. 779–785.

Kesler, Shelli R et al. (2016). "Atypical structural connectome organization and cognitive impairment in young survivors of acute lymphoblastic leukemia". In: *Brain connectivity* 6.4, pp. 273–282.

Klein, Arno et al. (2009). "Evaluation of 14 nonlinear deformation algorithms applied to human brain MRI registration". In: *Neuroimage* 46.3, pp. 786–802.

Lupo, Janine M et al. (2012). "7-Tesla susceptibility-weighted imaging to assess the effects of radiotherapy on normal-appearing brain in patients with glioma". In: *International Journal of Radiation Oncology* Biology* Physics* 82.3, e493–e500.

Ma, Qiongmin et al. (2016). "Radiation-induced functional connectivity alterations in nasopharyngeal carcinoma patients with radiotherapy". In: *Medicine* 95.29, e4275.

MATLAB (2015). *version 8.6 (R2015b)*. Natick, Massachusetts: The MathWorks Inc.

Melhem, Elias R et al. (2002). "Diffusion tensor MR imaging of the brain and white matter tractography". In: *American Journal of Roentgenology* 178.1, pp. 3–16.

Moldrich, Randal X et al. (2010). "Comparative mouse brain tractography of diffusion magnetic resonance imaging". In: *Neuroimage* 51.3, pp. 1027–1036.

Mori, Susumu et al. (1999). "Three-dimensional tracking of axonal projections in the brain by magnetic resonance imaging". In: *Annals of neurology* 45.2, pp. 265–269.

Mukherjee, P et al. (2008). "Diffusion tensor MR imaging and fiber tractography: theoretic underpinnings". In: *American journal of neuroradiology* 29.4, pp. 632–641.

Nagesh, Vijaya et al. (2008). "Radiation-induced changes in normal-appearing white matter in patients with cerebral tumors: a diffusion tensor imaging study". In: *International Journal of Radiation Oncology* Biology* Physics* 70.4, pp. 1002–1010.

Nasreddine, Ziad S et al. (2005). "The Montreal Cognitive Assessment, MoCA: a brief screening tool for mild cognitive impairment". In: *Journal of the American Geriatrics Society* 53.4, pp. 695–699.

Newman, Mark EJ (2003). "The structure and function of complex networks". In: *SIAM review* 45.2, pp. 167–256.

Onnela, Jukka-Pekka et al. (2005). "Intensity and coherence of motifs in weighted complex networks". In: *Physical Review E* 71.6, p. 065103.

Rubinov, Mikail and Olaf Sporns (2010). "Complex network measures of brain connectivity: uses and interpretations". In: *Neuroimage* 52.3, pp. 1059–1069.

Smith, Kristen M et al. (2014). "Reading skill in adult survivors of childhood brain tumor: A theory-based neurocognitive model." In: *Neuropsychology* 28.3, p. 448.

Smith, Stephen M (2002). "Fast robust automated brain extraction". In: *Human brain mapping* 17.3, pp. 143–155.

Sporns, Olaf, Giulio Tononi, and Rolf Kötter (2005). "The human connectome: a structural description of the human brain". In: *PLoS Comput Biol* 1.4, e42.

Sporns, Olaf et al. (2004). "Organization, development and function of complex brain networks". In: *Trends in cognitive sciences* 8.9, pp. 418–425.

Stupp, Roger et al. (2007). "Chemoradiotherapy in malignant glioma: standard of care and future directions". In: *Journal of Clinical Oncology* 25.26, pp. 4127–4136.

Tuch, David S (2004). "Q-ball imaging". In: *Magnetic resonance in medicine* 52.6, pp. 1358–1372.

Tymofiyeva, O et al. (2014). "Structural MRI connectome in development: challenges of the changing brain". In: *The British journal of radiology* 87.1039, p. 20140086.

Tzourio-Mazoyer, Nathalie et al. (2002). "Automated anatomical labeling of activations in SPM using a macroscopic anatomical parcellation of the MNI MRI single-subject brain". In: *Neuroimage* 15.1, pp. 273–289.

Wang, R et al. (2007). "Diffusion toolkit: a software package for diffusion imaging data processing and tractography". In: *Proc Intl Soc Mag Reson Med*. Vol. 15. 3720.

Watts, Duncan J and Steven H Strogatz (1998). "Collective dynamics of 'small-world'networks". In: *nature* 393.6684, pp. 440–442.

Publishing Agreement

It is the policy of the University to encourage the distribution of all theses, dissertations, and manuscripts. Copies of all UCSF theses, dissertations, and manuscripts will be routed to the library via the Graduate Division. The library will make all theses, dissertations, and manuscripts accessible to the public and will preserve these to the best of their abilities, in perpetuity.

Please sign the following statement:

I hereby grant permission to the Graduate Division of the University of California, San Francisco to release copies of my thesis, dissertation, or manuscript to the Campus Library to provide access and preservation, in whole or in part, in perpetuity.

9/6/16

Author Signature | Date